Journal of Catalysis 259 (2008) 174–182

Contents lists available at ScienceDirect

Journal of Catalysis

www.elsevier.com/locate/jcat

Preparation and catalytic properties of uniform particles of Ni_3Ge intermetallic compound formed inside the mesopores of MCM-41

T. Komatsu *, T. Kishi, T. Gorai

Department of Chemistry, Tokyo Institute of Technology, 2-12-1-E1-10 Ookayama, Meguro-ku, Tokyo 152-8550, Japan

ARTICLE INFO

Article history:
Received 11 April 2008
Revised 31 July 2008
Accepted 1 August 2008
Available online 6 September 2008

Keywords:
Intermetallic compound
Mesoporous silica
Nickel
Germanium
MCM-41
Nano-particle
Hydrogenation
Acetylene
Confinement effect

ABSTRACT

Uniform particles of Ni_3Ge intermetallic compound (IMC) were prepared inside the pores of MCM-41 mesoporous silica with various mesopore diameters. XRD and TEM revealed that Ni–Ge/MCM-41 thus prepared contained mainly fine metallic particles smaller than the pore size. IR spectra of adsorbed CO suggest the formation of a Ni–Ge IMC, probably Ni_3Ge, and the electron transfer from Ni to Ge. For H_2–D_2 equilibration, Ni_3Ge/MCM-41 had higher intrinsic activity than Ni/MCM-41 because of the high activity of Ni atoms at the corner and edge sites. Among MCM-41 and SiO_2 supports, those with smaller mesopores gave higher activity. The similar effect of pore size also was observed for the hydrogenation of cyclohexene. The difference in activity is discussed in terms of the confinement effect inside mesopores. For the hydrogenation of acetylene, Ni_3Ge gave higher ethylene selectivity than Ni because of the geometric and electronic effects through the formation of IMC.

© 2008 Elsevier Inc. All rights reserved.

1. Introduction

Intermetallic compounds (IMCs) are the stoichiometric compounds between two or more metal elements. In contrast to usual alloys, which are solid solution having the same crystal structure as that of either component metal, various IMCs have different specific crystal structures from their component metals. Therefore, some IMCs are known to have unique bulk properties, such as super conductivity, hydrogen storage ability, and so on. However, the catalytic properties of IMCs themselves have been little studied. One exception is the hydrogen storage compounds, such as $LaNi_5$ [1], which have been studied to investigate whether such an IMC has unique catalytic activity for hydrogenation and dehydrogenation reactions. The catalytic properties of unsupported IMCs without hydrogen storage ability have been reported more recently. In the hydrogenation of acetylene, CoGe [2], Ni_3Sn, and Ni_3Sn_2 [3] have higher selectivity to ethylene than Co and Ni. Pt_3Ge has higher selectivity to butenes than Pt in the hydrogenation of 1,3-butadiene [4]. Pt_3Ti shows higher activity than Pt for the hydrogenation of ethylene [5]. $CoHf_2$ shows high activity and stability in the CO_2 reforming of methane [6]. But because these catalysts consisted of large grains of IMCs with the size of 10–50 μm, their specific catalytic activity was very low compared with that of supported metal catalysts.

Supported IMC catalysts have been studied for several reactions. Many researchers have reported that Pt–Sn IMC phases are present in supported Pt–Sn bimetallic catalysts used for petroleum reforming; examples include $PtSn_4$, PtSn, and Pt_2Sn observed by microbeam diffraction [7] and Mössbauer spectroscopy [8]. But in usual bimetallic catalysts, neither the composition nor particle size of metallic species is uniform. Particles of several IMCs have differing stoichiometry, with pure metals and even oxidized species coexisting on the surface of supports. Consequently, the intrinsic catalytic properties of Pt–Sn IMCs have not been clarified sufficiently. Some researchers have attempted to prepare single-phase IMC particles on support oxide. Iwasa et al. [9] formed PdZn particles by reducing Pd/ZnO and found them active for the steam-reforming of methanol. Llorca et al. [7] prepared PtSn on SiO_2 by successive impregnation method. In earlier work, we prepared single-phase IMCs on the surface of SiO_2 [10]. Single-phase Ni–Sn IMCs have been prepared by chemical vapor deposition (CVD) of $Sn(CH_3)_4$ onto Ni/SiO_2 [11]. By changing CVD conditions, each IMC (Ni_3Sn, Ni_3Sn_2, and Ni_3Sn_4) was obtained as a single-phase compound. A similar method has been applied to other combination of metals to obtain RuTi/SiO_2 [12], Pd_3Bi/SiO_2 [13], and Pt_3Sn/H-SAPO-11 [14]; these IMCs did not have a uniform particle size, however. The definite characterization and assignment of active sites requires IMC particles of uniform size as well as composition. Moreover, the metal particles in uniform size will supply the

* Corresponding author. Fax: +81 3 5734 2758.
E-mail address: komatsu@chem.titech.ac.jp (T. Komatsu).

0021-9517/$ – see front matter © 2008 Elsevier Inc. All rights reserved.
doi:10.1016/j.jcat.2008.08.001

relationship between the coordination number and catalytic properties, especially in so-called "structure-sensitive" reactions. The roles of corner and edge atoms have been reported for pure metal catalysts, including Ni [15], Pt [16,17], and Rh [18].

Mesoporous materials consist of mesopores with uniform diameter. These ordered mesopores can provide unique spaces for the formation of metal particles with uniform size. In addition, the pore diameter can be easily varied using surfactant with different molecular sizes [19]. The accurate and stepwise control of occluded metal particle size can be achieved using such materials with regulated pore sizes. Incorporation of metals into the pores of mesoporous materials has been achieved in two ways, by direct synthesis and by postsynthesis. The direct synthesis approach is favorable to the higher dispersion of metals but is prone to collapsing the pore structure. In contrast, the postsynthesis approach is favorable for the retention of pore structure but is prone to depositing particles outside the pores. Szegedi et al. [20] prepared Ni-MCM-41 by the direct synthesis method, adding nickel chloride to the synthesis gel. For the postsynthesis method, an impregnation procedure is usually applied, for example, in the preparation of Pt/MCM-41 [21], Pt/FSM-16 [22], and Ni/MCM-41 [23]. Iwamoto and Tanaka [24] developed a template ion-exchange (TIE) method using MCM-41 before the removal of surfactant to incorporate metal cations inside the pores of MCM-41. Metal cations, such as Al, Ti, Cr, Mn, Zn and Zr, were successfully incorporated inside the mesopores as highly dispersed cations.

In the present study, we chose MCM-41 as a support for IMC particles because its mesopore diameter is small enough to obtain metal particles with high proportion of surface atoms. In addition, its mesopore diameter is easily manipulated by the size of surfactant. We chose the combination of Ni and Ge for the formation of IMC because in a preliminary work, Ni_3Ge supported on SiO_2 was found to be active for the partial hydrogenation of acetylene into ethylene in the presence of excess ethylene for the catalytic runs in a flow reaction system. This study's first aim was to obtain fine particles of single-phase Ni–Ge IMC, especially Ni_3Ge, with uniform particle diameter. The second purpose was to clarify the catalytic properties of small Ni_3Ge particles of uniform size. The electronic and geometric effects through the formation of IMC were evaluated through a comparison with Ni/MCM-41. The effect of mesopores of MCM-41 also were investigated through a comparison with Ni_3Ge supported on MCM-41 with various mesopore diameters and SiO_2.

2. Experimental

2.1. Catalyst preparation

MCM-41 mesoporous silica was prepared by hydrothermal synthesis as described previously [25]. The surfactant of cetyltrimethylammmonium bromide ($C_{16}H_{33}(CH_3)_3NBr$, 27 g) was dissolved into 270 g of pure water at 313 K. Colloidal silica (Nissan Chemical Ind., Snowtex 20, 159 g) and a 4.2% aqueous solution of sodium hydroxide (142 g) were dropped into the surfactant solution, and the mixture was stirred for 1 h. Then the mixture was transferred to an autoclave and heated at 413 K for 48 h without stirring. The solid thus obtained was filtered, washed with pure water, and dried at 353 K. Ni was introduced into this sample as described below. For the characterization of MCM-41 itself, the sample was further calcined in air at 813 K to obtain MCM-41(C16). Other MCM-41 samples were prepared in a similar manner using surfactants of dodecyltrimethylammonium bromide ($C_{12}H_{25}(CH_3)_3NBr$) or decyltrimethylammonium bromide ($C_{10}H_{21}(CH_3)_3NBr$). These were designated MCM-41(C12) and MCM-41(C10), respectively.

Introduction of Ni was carried out with TIE method [24]. For MCM-41(C16), the procedure was as follows. MCM-41 (10 g) containing surfactant was placed into 100 g of pure water. Nickel nitrate ($Ni(NO_3)_2{\cdot}6H_2O$, 0.91 g) was dissolved into 100 ml of pure water and dropped into the MCM-41 slurry and stirred for 1 h. TIE was carried out by keeping the slurry at 353 K for 20 h. The solid product was filtered, washed with pure water, and calcined at 813 K to obtain Ni/MCM-41(C16). Ni/MCM-41(C12) and Ni/MCM-41(C10) were prepared in a similar manner using 1.4 g and 1.0 g of nickel nitrate, respectively.

Ge was introduced by the CVD method in a similar manner to the preparation of Ni–Sn/SiO_2 [11]. Ni/MCM-41 (0.20 g) was placed into a quartz reactor (17 mm i.d.) and reduced in flowing hydrogen at 723 K for 1 h. After the temperature was set to an appropriate value, the vapor of $Ge(CH_3)_4$ saturated in flowing hydrogen at 273 K was introduced onto Ni/MCM-41 for a specific time as CVD treatment. The sample was further treated with pure hydrogen at 873 K for 1 h to obtain Ni–Ge/MCM-41.

As a reference catalyst, Ni_3Ge/SiO_2 was prepared stepwise through Ni/SiO_2 using silica gel (Caliact G6, Fuji Silysia). First, Ni(5 wt%)/SiO_2 was prepared by a usual pore-filling impregnation with an aqueous solution of nickel nitrate, followed by the calcination in air at 723 K and the reduction with flowing hydrogen at 723 K. Ge was then introduced by the CVD method similar to the preparation of Ni–Ge/MCM-41.

2.2. Characterization

The structural information of MCM-41 was obtained by the small-angle X-ray scattering (SAXS) technique using a Rigaku NANO-Viewer system with a Cu$K\alpha$ X-ray source. Nitrogen adsorption measurements were obtained with a Coulter SA-3100 instrument. The crystal structure of supported metal particles was examined by powder X-ray diffraction (Rigaku, RINT2400) with Cu$K\alpha$ X-ray. TEM images were obtained with a Jeol JEM-2010F microscope. The bulk composition of prepared catalysts was determined by ICP (Rigaku, JY38) after the samples were dissolved with HF solution and aqua regia.

The amount of adsorbed hydrogen was measured in a similar manner to the method reported by Freni et al. [26]. A small amount of catalyst was put into a quartz tube and reduced by flowing hydrogen at 723 K (873 K for Ni/MCM-41) for 1 h. After evacuation at 298 K, the sample was cooled to 195 K, after which H_2 (2 kPa) was introduced for 15 min and the sample was evacuated at 198 K. Then the sample was heated abruptly with a heating gun, and the evolved H_2 was analyzed by quadrupole mass spectrometry (Canon Anelva, M-101QA-TDM).

IR spectra of adsorbed CO were measured with a JASCO FT/IR-430 in its transmission mode. A self-supporting wafer (ca. 10 mg cm^{-2}) of catalyst was placed in a quartz cell with CaF_2 windows. After reduction in circulating hydrogen (15 kPa) at 723 K (873 K for Ni/MCM-41) for 1 h and evacuation at the same temperature, the sample was cooled in vacuo to 298 K. Then CO (1.5 kPa) was introduced at 298 K, and a spectrum was recorded. Spectra were obtained after evacuation at several temperatures.

2.3. Catalytic reaction

H_2–D_2 equilibration was carried out using a glass circulation system connected to a quadrupole mass spectrometer (Canon Anelva, M-101QA-TDM). Before each reaction, the catalyst was reduced for 1 h at 873 K for Ni/MCM-41 or at 723 K for other catalysts with 15 kPa of circulating H_2 followed by evacuation at the reduction temperature. A mixture of H_2 (6.7 kPa) and D_2 (99 at%, 6.7 kPa) was circulated through the catalyst at 273 K or 195 K. The

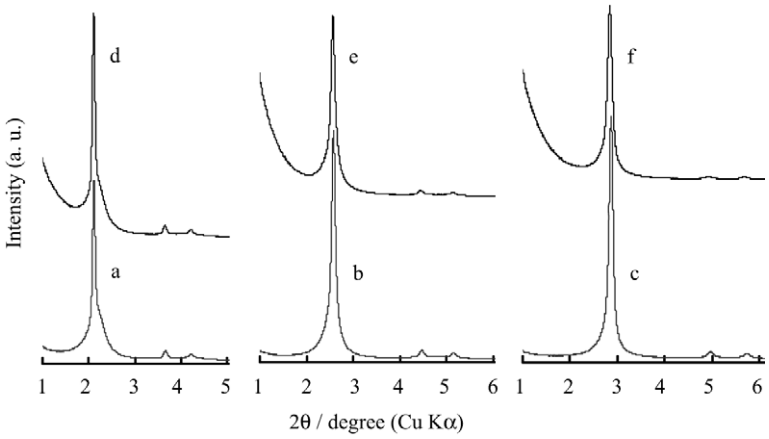

Fig. 1. SAXS patterns of MCM-41(C16) (a), MCM-41(C12) (b), MCM-41(C10) (c), Ni–Ge/MCM-41(C16) (d), Ni–Ge/MCM-41(C12) (e), Ni–Ge/MCM-41(C10) (f).

extent of the equilibration reaction was monitored by the change in the fraction of HD in hydrogen, $HD/(H_2 + HD + D_2)$.

The hydrogenation of acetylene was carried out in a continuous-flow reaction system under atmospheric pressure. A specific amount of catalyst was placed in a quartz tubular reactor (17 mm i.d.). Before the catalytic run, the catalyst was reduced with flowing hydrogen for 1 h at 873 K for Ni/MCM-41 or at 723 K for other catalysts. The reaction was started at 448 K or 523 K by supplying a reactant gas composed of C_2H_2 (14 kPa), H_2 (29 kPa), and He (balance) with a total flow rate of 28 ml min^{-1}. Gaseous products were analyzed with a Shimadzu GC-14B gas chromatograph with a flame ionization detector and a Varian CP8567 column. The selectivity to ethylene was calculated based on the total amount of carbon converted into ethylene. The hydrogenation of ethylene was carried out in a similar manner to the acetylene hydrogenation. The reaction was started at 353 K by supplying a reactant gas composed of C_2H_4 (25 kPa), H_2 (25 kPa), and He (balance) with a total flow rate of 80 ml min^{-1}.

The hydrogenation of cyclohexene was carried out in the continuous-flow reaction system under atmospheric pressure. A specific amount of catalyst was placed in a quartz tubular reactor (17 mm i.d.). Before the catalytic run, the catalyst was reduced with flowing hydrogen at 723 K for 30 min. The reaction was started at 363 K by supplying the vapor of cyclohexene (13 kPa) with a mixture of H_2 (29 kPa) and He (balance) with a total flow rate of 140 ml min^{-1}. Products were analyzed with a Shimadzu GC-8A gas chromatograph with a flame ionization detector and a column of Benton 34 and DIDP (GL Science).

3. Results and discussion

3.1. Characterization

To obtain particles of Ni–Ge IMCs with uniform diameter, we intended to form the particles inside the pores of the MCM-41 mesoporous silica. The particle diameter would be limited by the pore size of MCM-41. Furthermore, we prepared MCM-41 with various pore sizes using surfactants having alkyl chains of decyl (C10), dodecyl (C12), or hexadecyl (C16) groups to clarify the effect of particle diameter in nano-order. Fig. 1 shows SAXS patterns of such MCM-41 samples. All of the samples show typical SAXS patterns for an MCM-41 hexagonal structure. The peak position of (100) diffraction shifted to higher angle with decreasing alkyl chain length of surfactants from C16 (a) to C10 (c), indicating the narrower pore diameter for shorter alkyl chains [19]. From these patterns, the distances between the (100) planes (d_{100}), pore diameters [27], and wall thicknesses were obtained (Table 1). The pore diameters were in accordance with previous findings [28]. The wall thickness was almost constant for all of the MCM-41 samples. The dotted lines in Fig. 2 indicate the N_2 adsorption isotherms of three MCM-41 samples. A step at $P/P_0 = 0.15$–0.4 indicates the uniform mesopores. The shift in the step from 0.4 (C16) to 0.15 (C10) corresponds to the decreased mesopore diameter as revealed by the SAXS patterns (Fig. 1). Specific surface areas calculated by the BET method are listed in Table 1. The surface area of each MCM-41 was >900 $m^2\,g^{-1}$, indicating the presence of only negligible amorphous phases.

Table 1
Structural parameters and metal loadings of catalysts

Catalyst	d_{100} (nm)	Pore diameter (nm)	Wall thickness (nm)	BET surface area ($m^2\,g^{-1}$)	Ni loading (wt%)	Ni/Ge atomic ratio
MCM-41(C16)	4.20	3.4	0.8	947		
Ni/MCM-41(C16)				876	3.5	
Ni–Ge/MCM-41(C16)				760		3.1
MCM-41(C12)	3.49	2.6	0.9	972		
Ni/MCM-41(C12)				886	3.2	
Ni–Ge/MCM-41(C12)				807		2.9
MCM-41(C10)	3.14	2.3	0.8	962		
Ni/MCM-41(C10)				856	3.0	
Ni–Ge/MCM-41(C10)				572		3.0
Ni/SiO_2					2.5	
Ni_3Ge/SiO_2						3.0

The preparation of particles of Ni–Ge IMC inside the pores of MCM-41 was carried out by the CVD of $Ge(CH_3)_4$ on Ni/MCM-41. Ni was introduced into MCM-41 using the TIE technique [24], to avoid the formation of Ni particles on the external surface of MCM-41 crystallites. As shown in Table 1, Ni loadings were adjusted to ca. 3 wt%. CVD conditions, such as the temperature of Ni/MCM-41 and duration of CVD, were adjusted to obtain a Ni/Ge atomic ratio of 3, because we intended to form the IMC of Ni_3Ge, which has the widest composition range (22–25 at% Ni) of the Ni–Ge IMCs [29]. As shown in Table 1, the Ni/Ge ratios in the prepared catalysts were very close to 3.0. In the case of Ni–Sn IMCs on SiO_2 [11], Sn would be deposited selectively on the surface of Ni particles during the CVD of $Sn(CH_3)_4$ onto Ni/SiO_2, because little deposition of Sn onto pure SiO_2 occurred under the same conditions. For Ni–Ge, a similar selective deposition of Ge was observed for Ni/SiO_2; however, when $Ge(CH_3)_4$ was introduced onto the parent MCM-41, a comparable amount of Ge was deposited onto MCM-41. This indicates that on Ni/MCM-41, Ge atoms may be deposited onto both Ni particles and the pore walls of MCM-41 during CVD.

The effect of metal loading on the MCM-41 structure was examined. As shown in Figs. 1d, 1e and 1f, the (100) diffraction did not shift through the loading of Ni and Ge, suggesting that

the hexagonal structure was essentially retained during TIE, calcination, CVD, and reduction steps for every MCM-41 (although a significant change in low-angle baseline may have been caused by a decrease in structural regularity). Fig. 2 also shows the N_2 adsorption isotherms for Ni/MCM-41 and Ni–Ge/MCM-41. The height of the step decreased significantly for the metal-loaded samples, suggesting the slight decrease in adsorption capacity of mesopores. The specific surface areas (listed in Table 1) decreased significantly after the introduction of Ni and the subsequent addition of Ge. MCM-41(C10) exhibited the lowest surface area after the introduction of Ni–Ge. Because the hexagonal structure was retained, metal particles of similar size to the pore diameter might block some of the mesopores. The proportion of such particles would increase with decreasing mesopore diameter of the parent MCM-41.

Fig. 3 shows TEM images of Ni–Ge/MCM-41(C16) (a and b) and Ni/SiO_2 (c). Ni–Ge/MCM-41 (a) exhibits a one-dimensional pore structure characteristic of MCM-41, as expected based on Figs. 1 and 2. Although a small number of metal particles with diameters slightly larger than the pore diameter (3.4 nm) were found, most of the metal particles had diameters in the range of 2–3 nm, suggesting that the particles were located inside the mesopores of MCM-41. TEM images at higher magnification induced the destruction of mesopores of MCM-41. As shown in Fig. 3b, metal particles were found mainly on the external surface, probably because the particles were released out of the collapsed pores and adsorbed on the external surface of MCM-41 during the high-magnification measurement. These particles ranged in diameter from 2.8 to 3.4 nm. A particle size smaller than the pore diameter suggests that the metal particles were present inside the mesopores before the destruction of MCM-41 structure. On the other hand, the TEM image of Ni/SiO_2 (Fig. 3c) showed larger Ni particles with a wide diameter range (4–22 nm). The average diameter obtained from TEM was 8.2 nm, much larger than the metal particle size estimated for Ni–Ge/MCM-41(C16).

Metal species formed after Ge addition were examined by XRD, as shown in Fig. 4. Sharp diffraction peaks ($2\theta = 43.9°$ and 51.1°) assigned to Ni_3Ge were obvious for $Ni–Ge/SiO_2$ (b). No appreciable diffractions from Ni metal ($2\theta = 44.5°$) were observed. Clearly, the particles of single-phase Ni_3Ge were formed on SiO_2. Because the bulk composition was equal to $Ni/Ge = 3.0$, most of the Ni and Ge atoms formed Ni_3Ge. The average crystallite diameter was 10 nm. We designate this catalyst Ni_3Ge/SiO_2. On the other hand, Ni–Ge/MCM-41(C12) (a) exhibited no diffractions from metallic crystallites. XRD did not identify the metal particles, but revealed that their crystallite diameter must be smaller than 4 nm, as expected based on the TEM results (Fig. 3).

Hydrogen adsorption gives information about the surface of metal particles. We previously reported the adsorption of H_2 on Ni–Sn IMCs supported on SiO_2 [30]. The amount of adsorbed H_2 on Ni_3Sn/SiO_2 was one order of magnitude less than that on Ni/SiO_2, whereas the CO uptake on the former catalyst was as much as 77% of that on the latter catalyst. Ni_3Sn_4/SiO_2 did not adsorb any hy-

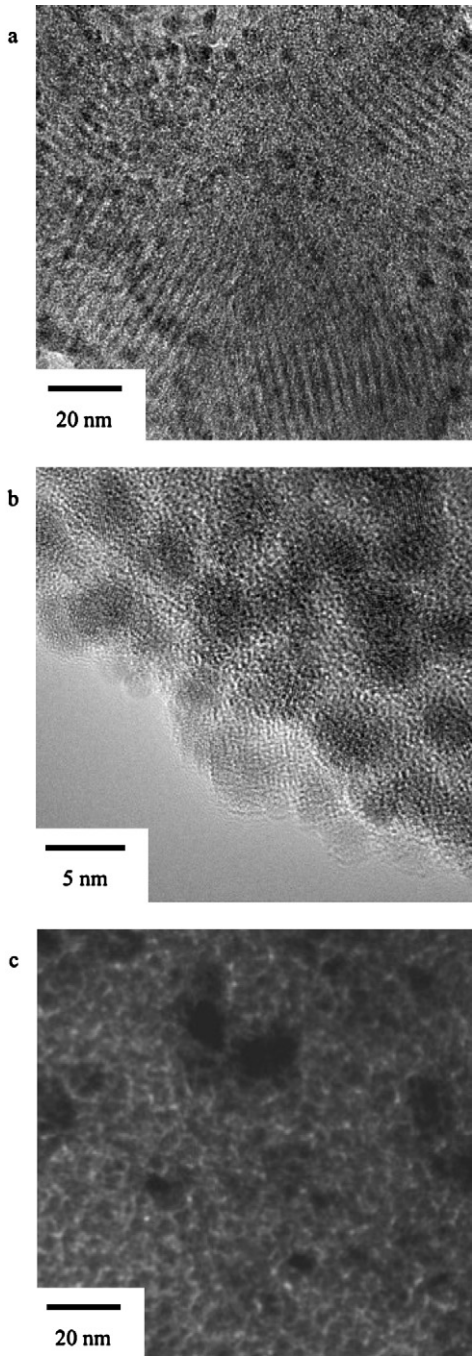

Fig. 3. TEM images of Ni–Ge/MCM-41(C16) (a, b) and Ni/SiO_2 (c).

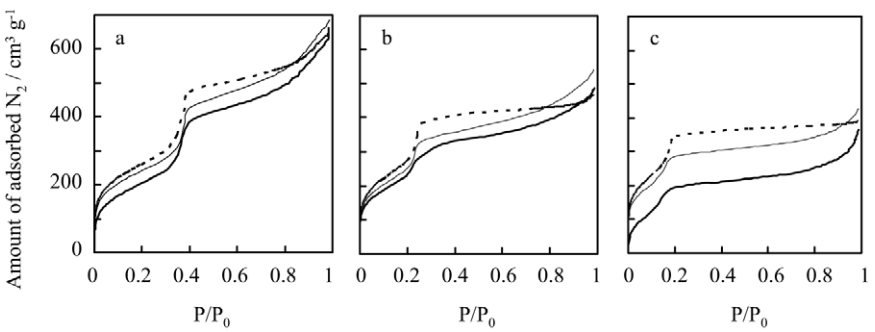

Fig. 2. N_2 adsorption isotherms on Ni–Ge supported (bold lines), Ni supported (thin lines) and parent (dotted lines) MCM-41(C16) (a), MCM-41(C12) (b) and MCM-41(C10) (c).

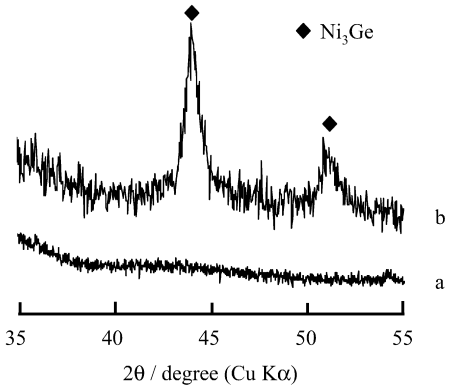

Fig. 4. XRD patterns of Ni–Ge/MCM-41(C12) (a) and Ni–Ge/SiO_2 (b) reduced at 873 K.

Table 2
H_2 adsorption data

Catalyst	Amount of adsorbed H_2 (mmol g_{Ni}^{-1})	Dispersion of Ni (%)	Average Ni diameter[a] (nm)
Ni/MCM-41(C16)	1.9	23	5.3
Ni–Ge/MCM-41(C16)	1.2		
Ni/MCM-41(C12)	2.3	27	4.6
Ni–Ge/MCM-41(C12)	0.90		
Ni/MCM-41(C10)	2.0	23	5.3
Ni–Ge/MCM-41(C10)	0.64		
Ni/SiO_2	0.91	11	12
Ni_3Ge/SiO_2	0.16		

[a] Assuming cubo-octahedron crystallites.

drogen. Dissociative adsorption of H_2 did not occur on the surface of Ni–Sn IMCs because of the long atomic distance between two adjacent Ni atoms compared with the situation on the surface of pure Ni. Table 2 gives the amount of adsorbed H_2 for Ni and Ni–Ge supported on MCM-41 and SiO_2. Ni/SiO_2 adsorbed 0.91 mmol g_{Ni}^{-1} of H_2. The dispersion of Ni was calculated as 11%, which corresponds to the average particle diameter of 12 nm assuming fcc cubo-octahedron crystallites. This value is not significantly different from the average particle size obtained from TEM (8.2 nm) and the average crystallite size obtained from XRD (10 nm). The H_2 uptake decreased to 0.16 mmol g_{Ni}^{-1} when Ni_3Ge was formed on SiO_2 similarly to Ni_3Sn/SiO_2 [30], indicating an increased atomic distance between Ni atoms through the formation of Ni_3Ge phase on the surface as well as in the bulk of particles. For Ni/MCM-41, the amount of H_2 adsorption (1.9–2.3 mmol g_{Ni}^{-1}) was about double of that on Ni/SiO_2, because of the smaller Ni particles on MCM-41; however, the average Ni diameters were 4.6–5.3 nm, larger than the estimated particle diameters for Ni–Ge/MCM-41 mentioned above. The partial blockage of mesopores by Ni particles will result in the decrease in H_2 uptake, making the apparent diameter larger. The addition of Ge decreased the H_2 uptake as in the case of Ni_3Ge/SiO_2, suggesting the formation of IMC, such as Ni_3Ge, in the pores of MCM-41. However, the extent of decrease in the H_2 uptake was not the same; the uptake on Ni_3Ge/SiO_2 was 18% of that on Ni/SiO_2, whereas the uptake on Ni–Ge/MCM-41(C12) was 39% of that on Ni/MCM-41(C12). We speculate that H_2 was adsorbed only on the edge and corner of Ni_3Ge crystallites. When Ni atoms form a cubo-octahedron crystallite, the proportion of edge and corner atoms to the total surface atoms is 10% for a 9-nm crystallite and 44% for a 2-nm crystallite [31]. The smaller crystallite has higher proportion of edge and corner atoms, leading to a smaller decrease in H_2 uptake from the formation of IMC, although the proportion of Ge atoms and the stoichiometry of H/Ni on edge and corner sites may affect H_2 uptake.

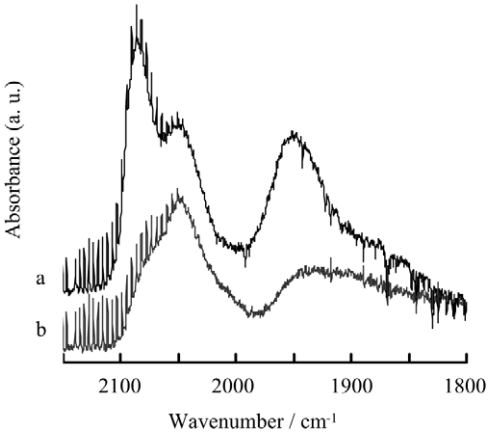

Fig. 5. IR spectra of CO adsorbed on Ni/MCM-41(C12) (a) and Ni/SiO_2 (b).

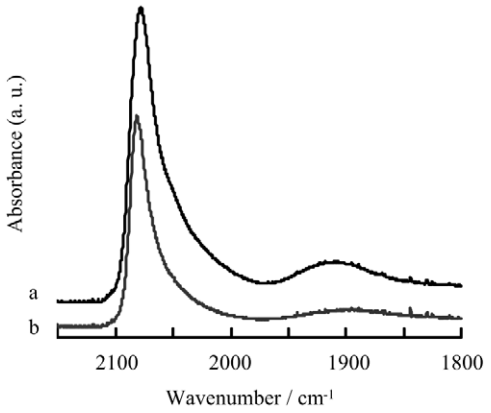

Fig. 6. IR spectra of CO adsorbed on Ni–Ge/MCM-41(C12) (a) and Ni_3Ge/SiO_2 (b).

Hydrogen adsorption measurements revealed the formation of an IMC-like surface on Ni–Ge particles inside the mesopores of MCM-41. We measured the IR spectra of adsorbed CO to characterize the Ni–Ge IMC. Fig. 5 shows IR spectra of CO adsorbed on Ni/MCM-41(C12) (a) and Ni/SiO_2 (b) under 1.5 kPa of CO. Ni/SiO_2 gave absorption bands at around 2050 and 1940 cm^{-1}, attributed to linear and bridged species, respectively. Ni/MCM-41(C12) gave similar bands, as well as an additional band at 2080 cm^{-1}. The additional band, which appeared on Ni/SiO_2 as a week shoulder, corresponds to the absorption by dicarbonyl species [32], probably adsorbed on Ni atoms on the edge and corner of crystallites. The strong absorption by dicarbonyl species again indicates the much smaller particle size of Ni inside MCM-41. Fig. 6 shows IR spectra of CO adsorbed on Ni–Ge/MCM-41(C12) (a) and Ni_3Ge/SiO_2 (b). In both spectra, absorption by bridged CO species at around 1900 cm^{-1} was drastically decreased compared with the Ni catalysts shown in Fig. 5. The similar disappearance of bridged species observed for Ni_3Sn/SiO_2 [30] and Pt_3Sn/H-SAPO-11 [14] can be attributed to the greater atomic distance between Ni or Pt atoms on the surface of these IMCs. The distance between neighboring Ni atoms on the (100) plane of Ni_3Ge was 0.357 nm, whereas that of pure Ni was 0.249 nm. The disappearance of bridged species provides further evidence for the formation of IMC in Ni–Ge/MCM-41.

To assign the IMC between Ni and Ge inside the mesopores of MCM-41, we investigated the CO species at higher wavenumbers. The strong absorption occurring at around 2080 cm^{-1} (Fig. 6) can be attributed to linear or dicarbonyl species. When the adsorbed CO was evacuated at higher temperatures, this band shifted to lower wavenumbers without splitting into two bands; therefore, this band can be attributed to the linear species. Fig. 7 shows

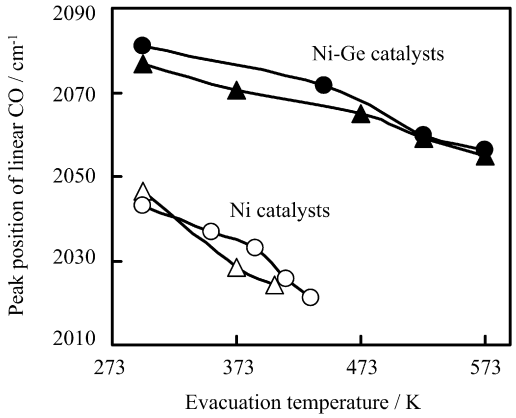

Fig. 7. Effect of evacuation temperature on IR peak position of linear CO species adsorbed on Ni–Ge/MCM-41(C12) (●), Ni_3Ge/SiO_2 (▲), Ni/MCM-41(C12) (○) and Ni/SiO_2 (△).

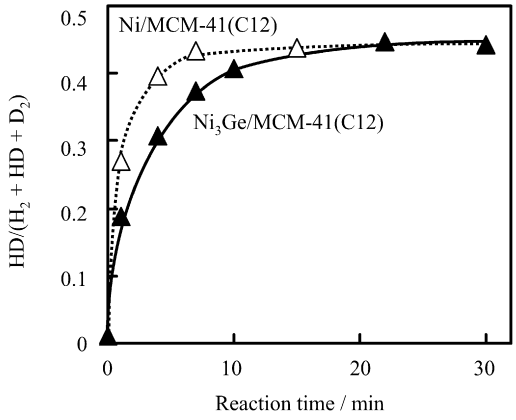

Fig. 8. H_2–D_2 equilibration at 273 K on Ni_3Ge/MCM-41(C12) (▲) and Ni/MCM-41(C12) (△).

the relationship between the peak position of this linear species and the evacuation temperature. The peak top shifted to lower wavenumbers on all the catalysts, indicating a decreased repulsive interaction between adjacent CO species. At high evacuation temperatures, the peak position should reflect the electronic state of Ni atoms bound to CO. Ni_3Ge/SiO_2 gave a higher wavenumber (2055 cm^{-1}) than Ni/SiO_2 (2025 cm^{-1}) at higher evacuation temperatures, indicating a stronger C–O bond and a weaker Ni–C bond on Ni_3Ge. This can be attributed to the lower electron density on Ni atoms in Ni_3Ge compared with pure Ni. For the MCM-41(C12)-supported catalysts, the peak positions were almost the same as those on the corresponding SiO_2-supported catalysts; therefore, the electronic state of Ni atoms on the surface of Ni–Ge particles on MCM-41 would be almost the same as that on the surface of Ni_3Ge on SiO_2. Based on these results, we conclude that particles of Ni_3Ge are formed inside the mesopores of MCM-41.

3.2. H_2–D_2 equilibration

To evaluate the ability of Ni_3Ge particles in the activation of hydrogen, H_2–D_2 equilibration was carried out in a closed reaction system. Fig. 8 shows the change in the fraction of HD in hydrogen with reaction time obtained at 273 K. On Ni/MCM-41(C12), HD was formed in the initial stage, and the fraction reached the equilibrium within 10 min. When the same amount of Ni_3Ge/MCM-41(C12) was used, HD was formed at a slightly lower rate than that on Ni/MCM-41(C12). We previously reported that for IMCs between transition and typical elements, such as CoGe [2], Ni_3Sn [3], and Pt_3Ge [4], the activity for H_2–D_2 equilibration is much lower than that of their component transition metals, Co, Ni, and Pt, respectively. We had to raise the reaction temperature by 150 K or more for these IMCs to obtain an HD formation rate comparable to that on these pure metals. Different from these IMCs, Ni_3Ge exhibited very high activity for hydrogen dissociation as an IMC which contains typical element. For the IMCs between two transition elements, however, $TiPt_3$ and Ti_3Pt exhibited greater activity than Pt [5]. The HD formation rate on $RuTi/SiO_2$ was only slightly lower than that on Ru/SiO_2 at the same temperature [12], suggesting that Ni_3Ge may have acted as an IMC between two transition metals for the activation of hydrogen.

Table 3
Reaction rate and TOF for H_2–D_2 equilibration at 273 K on Ni_3Ge and Ni catalysts

Catalyst	Initial rate (mmol s^{-1} g_{Ni}^{-1})	TOF (s^{-1})
Ni_3Ge/MCM-41(C12)	2.4	2.7
Ni_3Ge/SiO_2	0.019	0.062
Ni/MCM-41(C12)	3.3	0.72
Ni/SiO_2	0.14	0.076

The rate of HD formation was obtained from the initial slope of the HD formation curve. Table 3 compares the initial HD formation rates for the Ni_3Ge and Ni catalysts. As expected from Fig. 8, for MCM-41(C12)-supported catalysts, Ni_3Ge gave a HD formation rate as high as 73% of that on Ni. For SiO_2-supported catalysts, however, the rate on Ni_3Sn was 14% of that on Ni. It should be noted that the rate on Ni_3Ge/MCM-41(C12) was 130-fold greater than that on Ni_3Ge/SiO_2. This could be due to the effect of the smaller particle size of Ni_3Ge on MCM-41 despite the partial blockage of MCM-41 mesopores by Ni_3Ge. To investigate the intrinsic activity of surface Ni atoms, we calculated turnover frequency (TOF) for HD formation based on the amount of adsorbed H_2, as shown in Table 3. We neglected the catalytic activity of surface Ge atoms, because the activity of unsupported Ge powder for H_2–D_2 equilibration had been found to be very low compared with that of the powder of Co–Ge [2] and Pt-Ge [4] IMCs. For the Ni_3Ge catalysts, Ni_3Ge/MCM-41 gave about 40-fold greater TOF compared with Ni_3Ge/SiO_2. On both catalysts, hydrogen would be adsorbed on Ni at corner and edge sites, and HD formation would occur on the same Ni sites. Consequently, the large difference in TOFs can be explained by the difference in support structure. The confinement effect, first postulated for zeolite catalysis [33], has been reported for MCM-41 catalysts in the reactions of propylene oligomerization [34], cyclohexanone acetalization [35], *o*-xylene hydrogenation [21], and 1-hexene isomerization [36]. Compared with these reactants, the reaction of small hydrogen molecules can be accelerated by the narrow space between Ni_3Ge particles and mesopore wall. The Ni catalysts exhibited a similar enhanced TOF on MCM-41 (Table 3). For Ni crystallites, hydrogen was adsorbed on plane sites as well as edge and corner sites. With enhanced activity of Ni atoms at the latter sites, the increased TOF in Ni/MCM-41 can be attributed in part to the higher proportion of edge and corner sites owing to the smaller particles. For the MCM-41 catalysts, the higher TOF on Ni_3Ge/MCM-41 than that on Ni/MCM-41 can be explained by the contribution of less active Ni atoms at plane sites in Ni/MCM-41. On SiO_2, Ni had a slightly higher TOF than Ni_3Ge, however. If this can be attributed to the greater activity of edge and corner Ni on pure Ni compared with that on Ni_3Ge, then the highest TOF on Ni_3Ge/MCM-41 can be attributed to the support materials. The confinement effect would have the most significant effect on the activity of Ni_3Ge/MCM-41. The fact that Ni atoms that desorb hydrogen at 195 K were active for the reaction on Ni_3Ge/MCM-41, possibly resulting in overestimation of its TOF, cannot be neglected.

The effect of pore size was further studied for Ni_3Ge and Ni supported on MCM-41 with various mesopore diameters. H_2–D_2 equilibration was carried out at 195 K, a lower temperature than that reported in Table 3, to obtain accurate TOFs for the highly

Table 4
TOF for H_2–D_2 equilibration at 195 K on Ni_3Ge or Ni supported on various MCM-41

Support	TOF (s^{-1})	
	Ni_3Ge catalyst	Ni catalyst
MCM-41(C10)	0.15	0.079
MCM-41(C12)	0.089	0.017
MCM-41(C16)	0.049	0.015

Table 5
Conversion and selectivity in the hydrogenation of acetylene at 523 K and 1 h on stream

Catalyst	Acetylene conversion (%)	Selectivity (C-%)					
		CH_4	C_2H_4	C_2H_6	C_3H_6	C_4H_8	Others
Ni/MCM-41(C12)	16	1.1	67.8	7.0	6.2	12.6	5.3
Ni_3Ge/MCM-41(C12)	94	0.1	89.0	2.2	0.2	8.4	0.1

active catalysts. As shown in Table 4, on each MCM-41 support, the Ni_3Ge catalyst always had a higher TOF than the Ni catalyst, indicating the adsorption of hydrogen exclusively on highly active edge and corner Ni atoms on Ni_3Ge crystallites. Among the three Ni_3Ge catalysts, those supported on MCM-41(C10) gave the highest TOF. The same tendency was found for Ni catalysts. As mentioned above, if the confinement effect were more significant in the very narrow space, then the highest TOF on MCM-41(C10) catalysts could be explained by the stronger confinement effect. Because we prepared the Ni_3Ge from Ni/MCM-41, the particle size of Ni_3Ge would be slightly larger, due to the incorporation of Ge into the Ni crystallites. The space between the Ni_3Ge particles and mesopore wall would be narrower than that between the Ni particles and pore wall. The higher TOF on Ni_3Ge catalysts compared with Ni catalysts would be due in part to the stronger confinement effect in the narrower space in the Ni_3Ge/MCM-41 catalysts.

3.3. Hydrogenation of acetylene

We have reported that Co–Ge [2] and Ni–Sn [3] IMCs are selective catalysts for the formation of ethylene in the hydrogenation of acetylene. To clarify the catalytic activity and selectivity of Ni_3Ge fine particles, the hydrogenation of acetylene was carried out. The reactions were conducted with a flow reaction system instead of a closed circulation system, adopted to Co–Ge and Ni–Sn IMCs to gain insight into the catalyst's stability as well as its activity and selectivity. Table 5 shows the acetylene conversion and the selectivity to products obtained at 1 h on stream at a reaction temperature of 523 K. Ni/MCM-41(C12) gave a low acetylene conversion of 16%. The main product was ethylene, with selectivity of 68 C-%, and byproducts were mainly butenes, propylene, and ethane. The formation of coke and/or green oil [37] was observed on the catalyst after the reaction. The production of these large molecules at the initial stage of reaction deactivated surface Ni atoms, resulting in the low conversion. In contrast, Ni_3Ge/MCM-41(C12) gave a much higher conversion of 94% and a higher ethylene selectivity of 89 C-%. The selectivity to ethane was very low, indicating the retardation of deep hydrogenation compared with Ni/MCM-41(C12). The conversion decreased with time on stream down to 24% after 2.5 h. Formation of coke and/or green oil would occur gradually on this catalyst. In the case of Ni_3Ge/MCM-41(C10), however, the conversion did not decrease significantly; it remained >99% after 7 h on stream. Although the reason for the difference in stability between these Ni_3Ge/MCM-41 catalysts is not clear, Ni_3Ge/MCM-41(C10) was found to be stable in the partial hydrogenation of acetylene.

The effect of particle size of Ni_3Ge on the intrinsic activity was investigated based on the reaction results for Ni_3Ge supported on MCM-41(C12) and SiO_2. Fig. 9 shows the relationship between

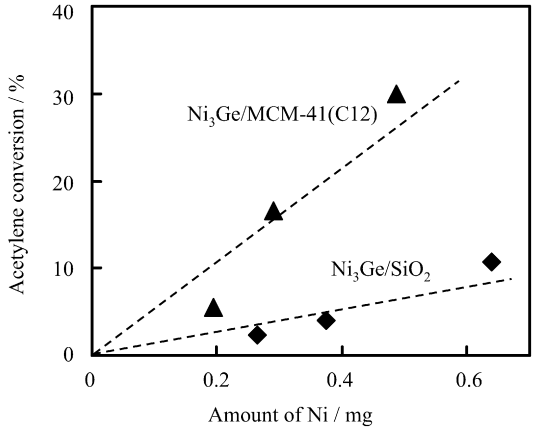

Fig. 9. Relation between acetylene conversion and the amount of Ni on Ni_3Ge/MCM-41(C12) (▲) and Ni_3Ge/SiO_2 (◆) obtained at 448 K and 1.5 h on stream.

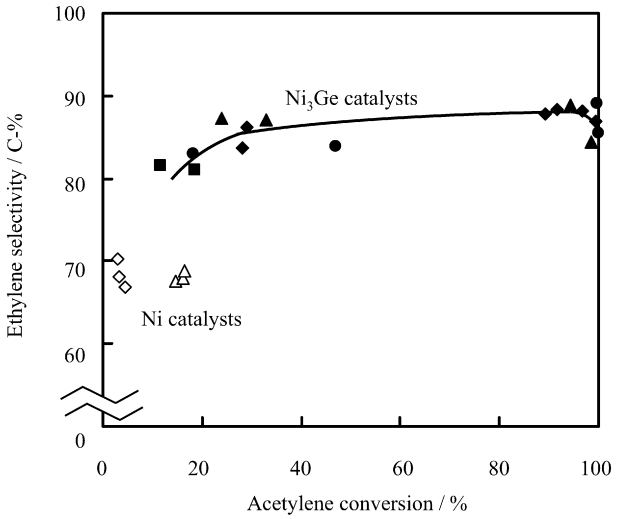

Fig. 10. Ethylene selectivity in the hydrogenation of acetylene at 523 K on Ni_3Ge supported on MCM-41(C10) (●), MCM-41(C12) (▲), MCM-41(C16) (■) and SiO_2 (◆), and on Ni/MCM-41(C12) (△) and Ni/SiO_2 (◇).

acetylene conversion at 1.5 h on stream and the amount of Ni in the catalysts. The reaction was carried out at a lower temperature, 448 K, to control the conversion and allow an accurate comparison of reaction rates. Ni_3Ge/MCM-41(C12) exhibited greater conversion than Ni_3Ge/SiO_2 with comparable amounts of Ni in the catalysts. This could be due to the smaller particle size of Ni_3Ge or to the greater dispersion of Ni, on MCM-41. Because hydrogen is adsorbed on Ni atoms on the edge and corner sites of Ni_3Ge, the active site for acetylene hydrogenation would be these Ni atoms or an ensemble of Ni atoms around the edge and corner. Based on the slopes of the dotted lines in Fig. 9, the conversion rates of acetylene per hydrogen adsorption site (edge or corner Ni) were calculated to be 0.83 $mol\,mol^{-1}\,s^{-1}$ for Ni_3Ge/MCM-41(C12) and 1.2 $mol\,mol^{-1}\,s^{-1}$ for Ni_3Ge/SiO_2. In contrast to H_2–D_2 equilibration, the mesopores of MCM-41 had no accelerating effect on acetylene hydrogenation.

Fig. 10 shows the relationship between the conversion of acetylene and the selectivity to ethylene obtained on various catalysts at a reaction temperature of 523 K. Ni_3Ge supported on three MCM-41 supports and SiO_2 gave a selectivity of 80–90 C-% in the wide conversion range of 10–100%, indicating almost the same selectivity at the same conversion. Clearly, the size of the Ni_3Ge crystallites and the pore diameter of the support had no appreciable influence on the selectivity for ethylene formation. In contrast, both Ni/MCM-41(C12) and Ni/SiO_2 had a selectivity ⩽70 C-% with

Table 6
Hydrogenation of cyclohexene at 363 K on Ni_3Ge catalysts

Catalyst	TOF (s^{-1})
Ni_3Ge/MCM-41(C10)	8.8
Ni_3Ge/MCM-41(C12)	7.5
Ni_3Ge/MCM-41(C16)	2.8
Ni_3Ge/SiO_2	0.67

acetylene conversion <20%. A geometric or electronic effect will result in greater selectivity of Ni_3Ge. The geometric effect will result from the difference in the atomic distance between adjacent Ni atoms, active sites. As mentioned above, the Ni_3Ge crystallites adsorbed less hydrogen than the Ni crystallites, indicating an expanding atomic distance between adjacent Ni atoms compared with pure Ni. A large atomic distance will retard the formation of ethylidyne species adsorbed in three-fold Ni sites. The ethylidyne species has been reported to be the intermediate for the direct hydrogenation of acetylene into ethane [37]; therefore, the formation of Ni_3Ge will retard the direct hydrogenation into ethane through ethylidyne. In addition, ethylene is known to be adsorbed on Ni surface as di-σ and π adsorbed species. The geometric effect of Ni_3Ge will retard the formation of di-σ species, which is more strongly adsorbed on Ni atoms. Therefore, on Ni_3Ge, ethylene will be adsorbed weakly as π species compared with pure Ni, which will be favorable to the ready desorption of ethylene without undergoing further hydrogenation into ethane.

The electronic effect also contributed to the high selectivity of Ni_3Ge. As mentioned above, IR spectra of adsorbed CO showed that the electron transfer from Ni to Ge in Ni_3Ge made the Ni atoms electron-deficient compared with pure Ni. In metal complexes with ethylene ligands, the back-donation of d-electron in metal into the antibonding orbital of ethylene strongly binds metal with ethylene. The lower electron density of Ni in Ni_3Ge weakens the adsorption of ethylene, preventing the deep hydrogenation into ethane. A similar electronic effect has been reported for Pt–Sn alloy, that is, the weak adsorption of ethylene due to decreased back-donation [38] and the low electron density of Pt compared with pure Pt [39]. Moreover, the electron-deficient Ni on Ni_3Ge will adsorb acetylene only weakly, to prevent oligomerization into larger molecules. We can conclude that the geometric and electronic effects both contribute to make Ni_3Ge a good catalyst for the selective hydrogenation of acetylene.

3.4. Hydrogenation of cyclohexene

To further study the effect of the narrow space inside mesopores and between particles and pore walls, the hydrogenation of the larger molecule (cyclohexene) was then carried out on Ni_3Ge catalysts at a reaction temperature of 363 K. Table 6 shows the TOFs obtained from the conversion of cyclohexene at 15 min on stream, along with the amount of adsorbed H_2. In all cases, the main product was cyclohexane, with selectivity >95 C-%. Ni_3Ge/SiO_2 had a lower TOF than any of the MCM-41 catalysts, due to the confinement effect similar to that observed for H_2–D_2 equilibration. However, compared with Ni_3Ge/SiO_2, the TOF for Ni_3Ge/MCM-41(C12) was 11-fold greater in this reaction and 44-fold greater in H_2–D_2 equilibration (Table 3). The impaired diffusion of larger cyclohexene molecules through the narrow space between Ni_3Ge particles and the pore wall may have affected the reaction rate. Among the Ni_3Ge/MCM-41 catalysts, MCM-41(C10) provided the highest TOF, as in the case of H_2–D_2 equilibration (Table 4), although the difference between MCM-41(C12) and MCM-41(C10) catalysts was not as great in the cyclohexene reaction. The presence of some Ni_3Ge particles inside MCM-41(C10) would make the space between the particles and the pore wall too narrow to allow diffusion of cyclohexene molecules.

4. Conclusion

Uniform particles of Ni–Ge IMC, Ni_3Ge, were formed inside the mesopores of MCM-41 through the successive loading of Ni and Ge. TIE with Ni^{2+} led to the presence of Ni particles inside the mesopores of MCM-41 with various pore diameters. Ni_3Ge was formed through the subsequent CVD of $Ge(CH_3)_4$ and H_2 treatment onto Ni/MCM-41 with no significant destruction of the mesopore structure. Most of the Ni_3Ge particles were located inside the mesopores and had a diameter no larger than the pore diameter of the MCM-41. Ni atoms on the edge and corner of Ni_3Ge crystallites adsorbed hydrogen. CO was weakly adsorbed on Ni_3Ge as a linear species compared with pure Ni. An electron transfer from Ni to Ge in Ni_3Ge made the Ni atoms electron-deficient.

Ni_3Ge/MCM-41 was found to have greater intrinsic activity than Ni/MCM-41 for H_2–D_2 equilibration and acetylene hydrogenation. Ni_3Ge is an exceptionally active IMC containing typical elements for the activation of hydrogen. Ni_3Ge exhibited greater selectivity to ethylene in acetylene hydrogenation compared with Ni, due to the expanded Ni–Ni atomic distance and decreased electron density of Ni atoms. Ni_3Ge/MCM-41(C10) exhibited very low activity for coke and green oil formation, resulting in the stable activity for acetylene hydrogenation. Compared with SiO_2-supported catalysts, Ni_3Ge supported on MCM-41 had much greater activity for H_2–D_2 equilibration and cyclohexene hydrogenation. This can be attributed in part to the confinement effect of narrow space between the Ni_3Ge particles and the pore walls. This confinement effect was more pronounced for MCM-41 with smaller mesopore diameters.

Acknowledgments

This work was partly supported by Grant-in-Aid for Creative Scientific Research from the Ministry of Education, Science and Culture, Japan. The authors thank Professor Iwamoto for help in preparing the Ni/MCM-41, Professor Asai for the SAXS measurements, and Mr. Genseki at the Center for Advanced Materials Analysis, Tokyo Institute of Technology, for the TEM measurements.

References

[1] W.E. Wallace, Chemtech 12 (1982) 752.
[2] T. Komatsu, M. Fukui, T. Yashima, Stud. Surf. Sci. Catal. 101 (1996) 1095.
[3] A. Onda, T. Komatsu, T. Yashima, Phys. Chem. Chem. Phys. 2 (2000) 2999.
[4] T. Komatsu, S. Hyodo, T. Yashima, J. Phys. Chem. B 101 (1997) 5565.
[5] T. Komatsu, D. Satoh, A. Onda, Chem. Commun. (2001) 1080.
[6] T. Komatsu, T. Uezono, J. Jpn. Petrol. Inst. 48 (2005) 76.
[7] J. Llorca, P.R. de la Piscina, J.L.G. Fierro, J. Sales, N. Homs, J. Catal. 156 (1995) 139.
[8] R. Bacaud, P. Bussiere, F. Figueras, J. Catal. 69 (1981) 399.
[9] N. Iwasa, S. Masuda, N. Ogawa, N. Takezawa, Appl. Catal. A 125 (1995) 145.
[10] T. Komatsu, A. Onda, Catal. Surv. Asia 12 (2008) 6.
[11] A. Onda, T. Komatsu, T. Yashima, J. Catal. 201 (2001) 13.
[12] T. Komatsu, Y. Fukui, Appl. Catal. A 279 (2005) 1730.
[13] T. Komatsu, K. Inaba, T. Uezono, A. Onda, T. Yashima, Appl. Catal. A 251 (2003) 315.
[14] T. Komatsu, H. Ikenaga, J. Catal. 241 (2006) 426.
[15] J.L. Carter, J.A. Cusumano, J.H. Sinfelt, J. Phys. Chem. 70 (1966) 2257.
[16] M. Boudart, A.W. Aldag, L.D. Ptak, J.E. Benton, J. Catal. 11 (1968) 35.
[17] J.P. Brunelle, A. Sugier, J.F. Le Page, J. Catal. 43 (1976) 273.
[18] J.H. Sinfelt, D.J.C. Yates, J. Catal. 8 (1967) 82.
[19] J.S. Beck, J.C. Vartuli, W.J. Roth, M.E. Leonowicz, C.T. Kresge, K.D. Schmitt, C.T.W. Chu, D.H. Olson, E.W. Sheppard, S.B. McCullen, J.B. Higgins, J.L. Schlenker, J. Am. Chem. Soc. 114 (1992) 10834.
[20] Á. Szegedi, M. Popova, V. Marvrodinova, M. Urbán, I. Kiricsi, C. Minchev, Microporous Mesoporous Mater. 99 (2007) 149.
[21] F. Letellier, J. Blanchard, K. Fajerwerg, C. Louis, M. Breysse, D. Guillaume, D. Uzio, Catal. Lett. 110 (2006) 115.

[22] A. Fukuoka, J. Kimura, T. Oshio, Y. Sakamoto, M. Ichikawa, J. Am. Chem. Soc. 129 (2007) 10120.
[23] X. Li, W. Ji, J. Zhao, S. Wang, C. Au, J. Catal. 236 (2005) 181.
[24] M. Iwamoto, Y. Tanaka, Catal. Surv. Jpn. 5 (2001) 25.
[25] T. Abe, T. Tachibana, T. Uematsu, M. Iwamoto, J. Chem. Soc. Chem. Commun. (1995) 1617.
[26] S. Freni, S. Cavallaro, N. Mondello, L. Spadaro, F. Frusteri, J. Power Souces 108 (2002) 53.
[27] Y. Tominaga, S. Igawa, S. Asai, M. Sumita, Electrochim. Acta 50 (2005) 3949.
[28] S.K. Jana, A. Mochizuki, S. Namba, Catal. Surv. Jpn. 8 (2004) 1.
[29] Binary Alloy Phase Diagrams, second ed., ASM International and National Institute of Standards and Technology, 1990.
[30] A. Onda, T. Komatsu, T. Yashima, J. Catal. 221 (2003) 378.
[31] R. Van Hardeveld, F. Hartog, Surf. Sci. 15 (1969) 189.
[32] C.H. Bartholomew, R.B. Pannell, J. Catal. 65 (1980) 390.
[33] E.G. Derouane, J.M. Andre, A.A. Lucas, J. Catal. 110 (1988) 58.
[34] G. Belusgi, C. Perego, A. Carati, S. Peratello, E. Previde Massara, G. Perego, Stud. Surf. Sci. Catal. 84 (1994) 85.
[35] M. Iwamoto, Y. Tanaka, N. Sawamura, S. Namba, J. Am. Chem. Soc. 125 (2003) 13032.
[36] S. Pariente, P. Trens, F. Fajula, F. Di Renzo, N. Tanchoux, Appl. Catal. A 307 (2006) 51.
[37] Á. Molnár, A. Sárkány, M. Varga, J. Mol. Catal. A Chem. 173 (2001) 185.
[38] Y.A. Ryndin, C.C. Santini, D. Prat, J.M. Basset, J. Catal. 190 (2000) 364.
[39] J.A. Rodriguez, S. Chaturvedi, T. Jirsak, J. Hrbek, J. Chem. Phys. 109 (1998) 4052.